Oct 23rd, 12:00 AM

A Study of Cold-formed Z-section Steel Members under Axial Loading

Rene W. Purnadi

John L. Tassoulas

Dimos Polyzois

Tenth International Specialty Conference on Cold-formed Steel Structures
St. Louis, Missouri, U.S.A., October 23-24, 1990

A STUDY OF COLD-FORMED Z-SECTION STEEL MEMBERS UNDER AXIAL LOADING

By

René W. Purnadi [1], John L. Tassoulas [2],
and Dimos Polyzois [3]

INTRODUCTION

Cold-formed steel members are becoming increasingly popular because of their relatively high strength-to-weight ratio. Typically, they find applications in lightweight structures, e.g., purlins, bracing members and columns for industrial racks. The load-carrying capacity of cold-formed members depends strongly on the shape of their cross section. Figure 1 identifies the geometric parameters of the Z section examined in the present work. Due to the relative ease of the manufacturing process, many shapes are cold-formed from steel plates. This results in rather thin members which are more susceptible to local and distortional buckling (see Figure 2). However, local buckling does not necessarily imply failure of the member, since, usually, there is considerable postbuckling strength. On the other hand, distortional buckling, due to inadequate stiffening, reduces the postbuckling capacity significantly. The Z section offers an additional incentive: if the angle between the lip (stiffener) and the flange is less than 90°, Z-zection members can be stacked on each other for ease of transportation.

The 1986 AISI (American Iron and Steel Institute) Specification covers all shapes of cross sections, including Z sections. Prior to the work carried out at The University of Texas at Austin, there had been no experimental verification of the Specification for Z sections. In fact, this lack of information regarding the performance of Z-section members motivated the present study. Specimens with a variety of lengths, lip angles and load eccentricities along the web were tested. Of course, the limited number of specimens prohibited a thorough study of all parameters affecting the behavior of Z-section

[1] Graduate Student, Department of Civil Engineering, The University of Texas, Austin, Texas 78712-1076.

[2] Associate Professor, Department of Civil Engineering, The University of Texas, Austin, Texas 78712-1076.

[3] Associate Professor, Department of Civil Engineering, University of Manitoba, Winnipeg, Manitoba, Canada.

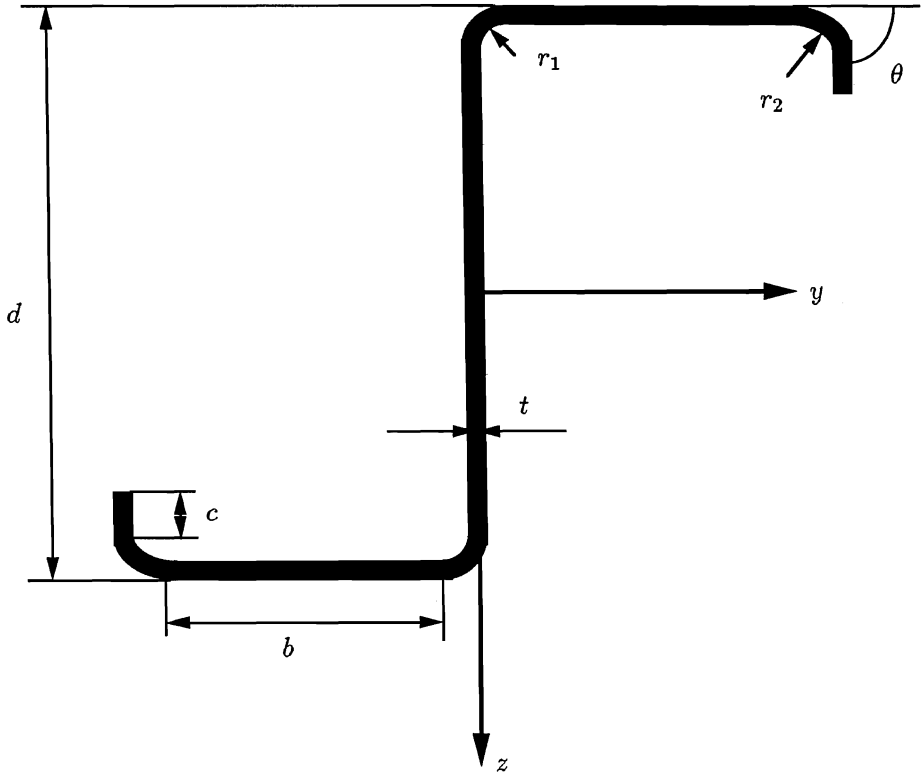

d = overall height (4.0 in)
b = flange width (2.0 in)
c = lip width (0.65 in)
t = thickness (0.08 in)
r_1 = radius of flange-web junction (0.2 in)
r_2 = radius of flange-lip junction
θ = lip angle

Figure 1: Geometry of the Z section

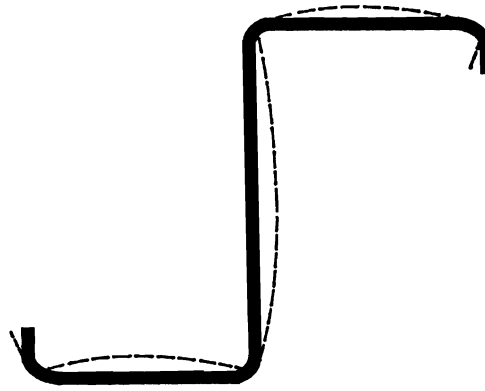

Figure 2: (a) Local buckling

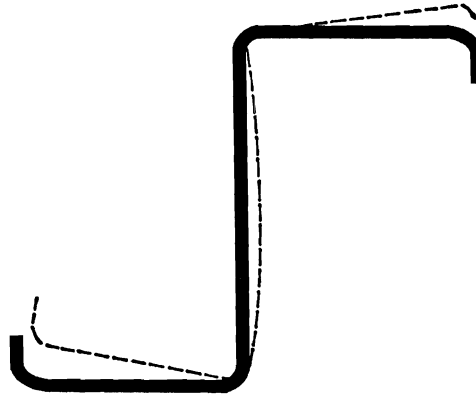

Figure 2: (b) Distortional buckling

Table 1: List of specimens tested (numbers in parentheses indicate numbers of specimens tested)

Specimen Length	Eccentricity	Lip Angle			
in	in	0°	30°	50°	80°
18	0.0	(6)	(6)	(4)	(3)
36	0.0	(2)	(2)	(2)	(2)
	$e_z = 1.0$	(1)	(1)	(1)	(1)
	$e_z = 2.0$	(1)	(1)	(1)	(1)
	$e_z = 3.0$	(1)	(1)	(1)	(1)
60	0.0	(2)	(2)	(2)	(2)
	$e_z = 1.0$	(1)	(1)	(1)	(1)
	$e_z = 2.0$	(1)	(1)	(1)	(1)
	$e_z = 3.0$	(1)	(1)	(1)	(1)
96	0.0	(2)	(4)	(2)	(3)
	$e_z = 1.0$	(1)	(1)	(1)	(1)
	$e_z = 2.0$	(1)	(1)	(1)	(1)
	$e_z = 3.0$	(1)	(1)	(1)	(1)

members. Therefore, a complementary analytical investigation was undertaken which confirmed the experimental findings and provided additional data on the importance of parameters not explored in the laboratory tests, namely, the yield stress of the steel used, the higher yield stress at corners of the cold-formed cross section, the initial imperfection of the members and the eccentricity of the load in directions normal and parallel to the web.

EXPERIMENTAL STUDY

Specimens

There were 46 specimens tested under concentric load and 36 specimens under eccentric loads (Table 1). The cross-section area was practically the same for all specimens. The web was about twice the flange. Thus, with adequate stiffening of the flange by the lip, if local buckling were to occur, it would be initiated in the web. Several lengths of specimens were selected. The shortest, $18in$, specimens would fail by a combination of local buckling and yielding. The $36in$ and $60in$ specimens would reach ultimate strength by some combination of local buckling and overall buckling in the plastic range. Finally, the long, $96in$, specimens would exhibit overall buckling in the elastic range, which might be preceded by local buckling. The yield stress (F_y) of the steel was obtained from coupon tests. For all practical purposes,

the yield stress was found to be about $40.6ksi$ in most of the specimens and approximately $57.0ksi$ in the rest. The conditions imposed on the ends of the specimens were such that rotations were allowed with respect to all axes, but translation was permitted only in the longitudinal direction. A unique ball-and-socket fixture (see Figure 3) was attached to the testing machine. The ball was engaged to an end plate by means of a small drilled conical trench. The specimens were attached to the other side of the end plate: they were placed in Z grooves on the end plates (see Figure 4) for concentric loading, or they were welded to the end plates for eccentric loading cases. The position of the centroid of the specimen with respect to the conical trench measured the eccentricity. Warping at both ends was prevented by the end plates.

Equipment and Instrumentation

The short specimens, $18in$ and $36in$, were tested in a standard $60kip$ hydraulic machine. Because of the limited available space in the standard $60kip$ machine, a test frame, equipped with a manual hydraulic pump, was used for the longer, $60in$ and $96in$, specimens. Linear transducers were used for continuous monitoring of the axial displacement for $18in$ specimens, the axial displacement and lateral displacement perpendicular to the web at the centroid of the middle cross section for $36in$ specimens and the lateral displacements in both directions at the centroid of the middle cross section for $60in$ and $96in$ specimens. These transducers were connected to plotters for graphical output. Also, dial gages were installed on the end plates so as to measure the rotations of the end cross sections. The standard $60kip$ machine had its own converter from load to electric impulse transmitted to the plotters. In the test frame, the manual hydraulic pump was connected to a pressure transducer which, with the help of a power supply, converted the hydraulic pressure to an electric impulse sent to the plotters. The conversion from hydraulic pressure to load was achieved through calibration of the pump using the standard $60kip$ machine.

Procedure

The specimens were whitewashed before being tested. The whitewash served as an indicator of the occurrence and extent of yielding by peeling off during testing of the specimens. Local buckling was evidenced by ripples on the surface of the specimens. For short specimens, the visual observation was aided by a straight metal ruler which was slid along various parts of the specimens in order to reveal the initiation of a local buckle. The load was applied at a rate of about $1kip/min$.

Results

The experimental results are given in Tables 2-5 together with the estimates of the ultimate load based on the 1986 AISI Specification. Only specimens with 0° lip angle exhibited obvious ripples indicative of early local buckling. Specimens with a 30° lip angle experienced slight distortion: the flange and lip rotated with respect to the web. Apparently, specimens with 50° and 80° lip angles were adequately stiffened and their cross sections did not undergo any deformation.

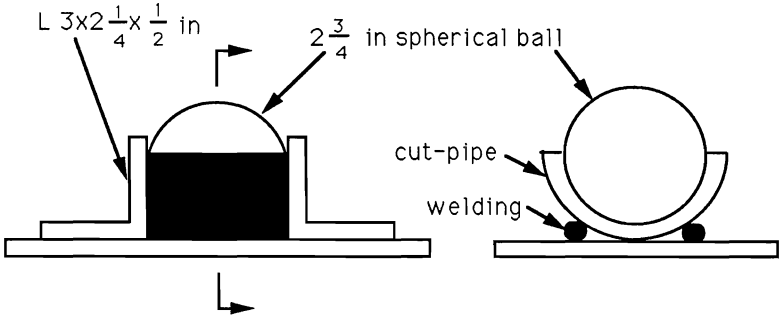

Figure 3: Ball-and-socket fixture

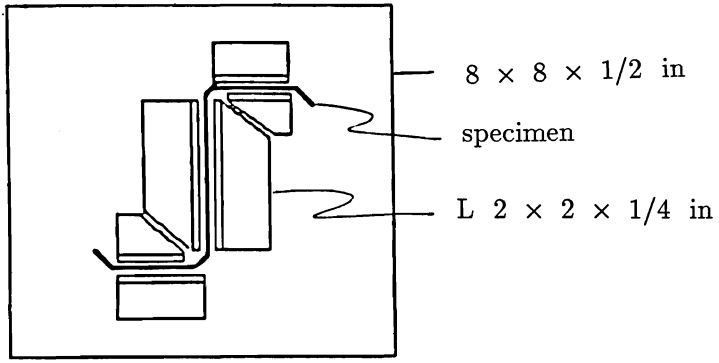

Figure 4: Z groove on end plate

Table 2: Comparison of experimental results and AISI estimates for $18in$ specimens

Specimen[1]	AISI estimated strength, kips	Experimental result kips	The ratio $\frac{P_{AISI}}{P_{test}}$
$18, 0°$ #1[2]	7.726	25.50	0.303
$18, 0°$ #2[2]	7.976	24.30	0.328
$18, 0°$ #3	6.856	17.65	0.389
$18, 0°$ #4	6.121	17.10	0.358
$18, 0°$ #5	5.643	19.00	0.297
$18, 0°$ #6	5.643	17.35	0.325
$18, 30°$ #1	27.427	24.60	1.115
$18, 30°$ #2	27.938	25.30	1.104
$18, 30°$ #3[2]	36.266	35.00	1.036
$18, 30°$ #4[2]	35.641	34.05	1.047
$18, 30°$ #5	26.580	23.55	1.129
$18, 30°$ #6	26.580	25.10	1.059
$18, 50°$ #1	32.063	34.60	0.927
$18, 50°$ #2	31.079	34.10	0.911
$18, 50°$ #3	31.156	34.90	0.893
$18, 50°$ #4	31.291	34.60	0.904
$18, 80°$ #1	32.759	34.35	0.954
$18, 80°$ #2	30.032	31.30	0.959
$18, 80°$ #3	32.278	36.55	0.883

[1] $F_y = 42.0$ ksi
[2] $F_y = 58.0$ ksi

Table 3: Comparison of experimental results and AISI estimates for $36in$ specimens

Specimen[1]	AISI estimated strength, kips	Experimental result kips	The ratio $\frac{P_{AISI}}{P_{test}}$
36, 0° #1	7.086	22.35	0.317
36, 0° #5	7.132	23.35	0.305
36, 30° #1	32.816	32.50	1.009
36, 30° #5	33.045	32.80	1.007
36, 50° #1	36.255	35.05	1.034
36, 50° #5	35.565	35.25	1.009
36, 80° #1	37.700	35.85	1.051
36, 80° #5	36.554	32.90	1.111
Eccentric Loading, e = 1.0 in.			
36, 0° #2	4.519	14.25	0.317
36, 30° #2	14.866	17.70	0.841
36, 50° #4	16.766	19.05	0.880
36, 80° #2	17.013	18.35	0.927
Eccentric Loading, e = 2.0 in.			
36, 0° #3	3.803	10.05	0.378
36, 30° #3	11.102	11.60	0.957
36, 50° #3	12.381	12.70	0.975
36, 80° #3	12.562	12.20	1.030
Eccentric Loading, e = 3.0 in.			
36, 0° #4	3.282	8.00	0.410
36, 30° #4	9.260	8.85	1.046
36, 50° #2	10.196	8.85	1.152
36, 80° #4	10.310	9.45	1.091

[1] F_y = 58.0 ksi

Table 4: Comparison of experimental results and AISI estimates for $60in$ specimens

Specimen[1]	AISI estimated strength, kips	Experimental result kips	The ratio $\frac{P_{AISI}}{P_{test}}$
60, 0° #1	6.993	15.26	0.458
60, 0° #5	7.367	19.12	0.385
60, 30° #1	26.443	29.55	0.895
60, 30° #5	26.927	28.98	0.929
60, 50° #1	28.577	30.85	0.926
60, 50° #5	29.298	29.00	1.010
60, 80° #1	28.415	30.06	0.945
60, 80° #5	27.979	28.73	0.974
Eccentric Loading, e = 1.0 in.			
60, 0° #2	4.333	10.89	0.398
60, 30° #2	12.922	12.50	1.034
60, 50° #2	13.746	13.68	1.005
60, 80° #2	13.789	13.64	1.011
Eccentric Loading, e = 2.0 in.			
60, 0° #3	3.554	8.39	0.424
60, 30° #3	10.016	9.85	1.017
60, 50° #3	10.644	9.48	1.123
60, 80° #3	10.674	9.69	1.101
Eccentric Loading, e = 3.0 in.			
60, 0° #4	3.271	6.86	0.477
60, 30° #4	8.110	8.04	1.009
60, 50° #4	8.453	7.53	1.123
60, 80° #6	8.578	7.75	1.107

[1] F_y = 58.0 ksi

Table 5: Comparison of experimental results and AISI estimates for $96in$ specimens

Specimen[1]	AISI estimated strength, kips	Experimental result kips	The ratio $\frac{P_{AISI}}{P_{test}}$
96, 0° #1	5.687	11.31	0.503
96, 0° #5	6.104	10.10	0.604
96, 30° #1	12.122	16.44	0.737
96, 30° #2	12.227	13.34	0.917
96, 30° #7	12.168	13.69	0.889
96, 30° #8	12.214	14 79	0.826
96, 50° #1	12.244	14.46	0.847
96, 50° #2	12.075	14.47	0.834
96, 80° #1	11.524	15.55	0.741
96, 80° #2	11.524	13.22	0.872
96, 80° #6	11.593	13.99	0.828
Eccentric Loading, e = 1.0 in.			
96, 0° #3	3.562	5.60	0.636
96, 30° #3	6.672	6.92	0.964
96, 50° #3	6.799	6.99	0.982
96, 80° #3	6.511	6.80	0.957
Eccentric Loading, e = 2.0 in.			
96, 0° #6	2.890	4.78	0.604
96, 30° #4	5.316	5.46	0.973
96, 50° #4	5.312	5.53	0.961
96, 80° #4	5.221	5.34	0.978
Eccentric Loading, e = 3.0 in.			
96, 0° #5	2.429	3.96	0.613
96, 30° #5	4.459	4.40	1.013
96, 50° #5	4.714	4.50	1.048
96, 80° #5	4.368	4.81	0.913

[1] F_y = 42.0 ksi

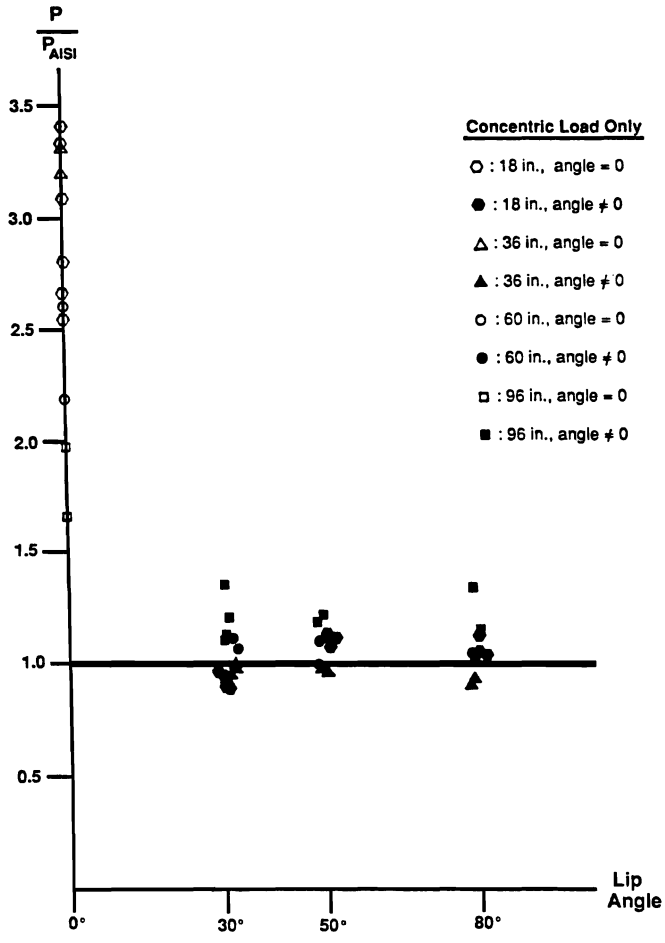

Figure 5: Comparison of experimental results with AISI estimates; concentric load

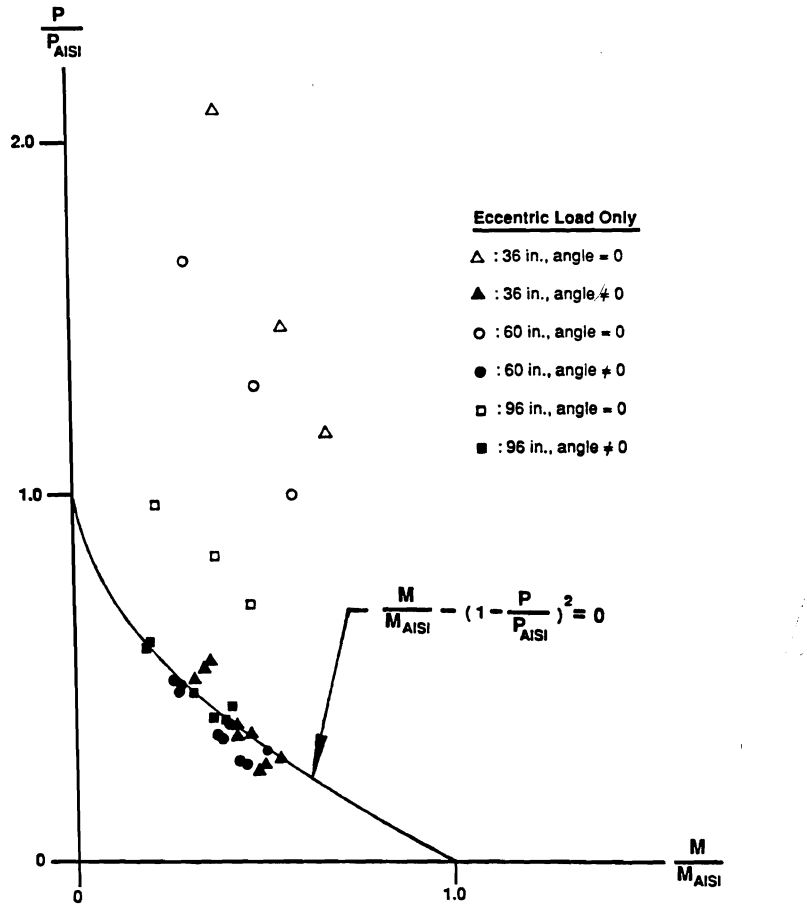

Figure 6: Comparison of experimental results with AISI estimates; eccentric loads

The ultimate loads for specimens (of the same length) with 30°, 50° and 80° lip angles are reasonably close to each other, significantly higher than with 0° lip angle. Comparison (Tables 2-5) with the load capacities estimated according to the 1986 AISI Specification indicates good agreement for specimens with nonzero lip angles. AISI estimates for specimens with 0° lip angle are seen to be very conservative. Equation C4-5 of the Specification considers the stress at which local buckling may occur as the maximum stress that an unstiffened element can carry, ignoring the additional capacity beyond local buckling. In addition, equation C4-5 assumes that there is no rotational stiffness at the web-to-flange junction. Figure 5 shows the ratio of the measured ultimate load to the AISI estimate plotted versus the lip angle for specimens subjected to concentric loads. For eccentric loads (combined axial force and moment), equation C5-1 of the Specification applies. Figure 6 depicts the results for specimens subjected to eccentric loads in comparison with the AISI estimates. From Figures 5 and 6, it is clear that the critical local buckling stress substantially underestimates the maximum stress that an unstiffened element can be subjected to. In fact, if equation C4-5 of the Specification is not adhered to, the ratio P_{AISI}/P_{test} is increased from $0.311 - 0.554$ to $0.829 - 1.082$ for concentric loads, and from $0.369 - 0.618$ to $0.774 - 0.813$ for eccentric loads.

ANALYTICAL STUDY

The results of the experimental study, although limited by the number of available specimens, furnished important information regarding the performance of Z-zection members under axial loads. Towards further understanding of the behavior of cold-formed members, a technique was developed on the basis of the finite element method and applied to the analysis of the specimens tested in the laboratory. After the validity of the technique was established, additional results were obtained on the behavior of Z-section members. The technique and the analytical results are summarized below.

Analytical Technique

The analytical technique is based on a Lagrangian description of the member with the initial undeformed configuration of the member serving as the reference configuration. The description makes use of a net of coordinate lines embedded in and deforming with the member. This so-called convected-coordinate formulation has been discussed in detail by Needleman (1982) for arbitrary continua. Specifics of its application to the structural members of interest in the present study are given by Purnadi (1990). Steel is assumed to be an elastoplastic, hardening material. The constitutive equations are those of the J_2 flow theory of plasticity with isotropic hardening.

The member is discretized using the 9-node isoparametric shell finite element (see Figure 7), originally developed for linear analysis of shells by Ahmad et al. (1970). The adaptation of the element to nonlinear analysis on the basis of the convected-coordinate formulation is described by Purnadi

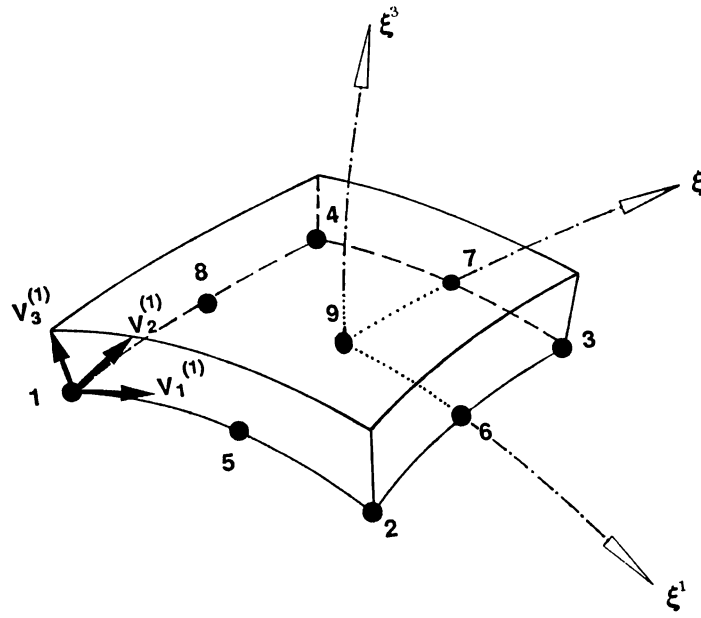

Figure 7: 9-node isoparametric shell finite element

(1990). Reduced integration is applied to the evaluation of the stiffness matrix and load vector of the element: a 2 by 2 instead of a 3 by 3 array of Gauss-Legendre integration points are used over any lamina of the element. The spurious modes of deformation which result from this underintegration are prevented by the boundary conditions in the problems of interest in the present study and the element performs remarkably well. The number of integration points through the thickness of the element depends on the extent of yielding. In all calculations performed in this work, 5 Gauss-Legendre integration points were found to be adequate.

The numerical integration of the elastoplastic constitutive equations is carried out using the well known radial return method, widely used in small-strain plasticity. The large-deformation modification of the method is described by Purnadi (1990).

Finally, it should be mentioned that most of the Z-section members considered were analyzed by specifying increments of the axial displacement of one of the ends and monitoring the axial force required for equilibrium up to and slightly past the limit point (peak value of the axial force). However, this approach failed in some cases characterized by a "sharply turning" equilibrium curve beyond the limit point. In these cases, the Riks method (Riks 1984) of advancing the solution along the equilibrium curve was employed.

Results

Figure 8 depicts the mesh of finite elements for one of the test specimens analyzed; a deformed configuration slightly beyond ultimate strength

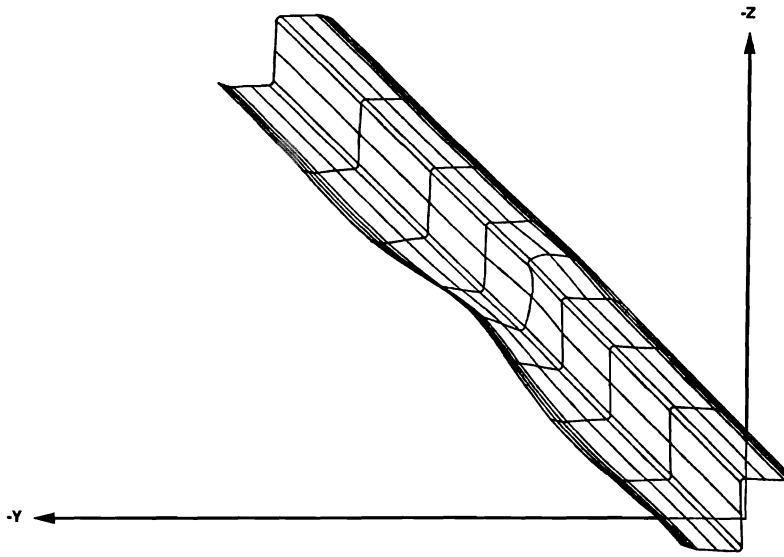

Figure 8: Mesh of finite elements for $36in$ specimen ($F_y = 57.0ksi$) with 20° lip angle under eccentric load ($e_z = 2.0in$); deformed configuration slightly beyond ultimate strength

is shown. It can be seen that the discretization is capable of capturing local buckling very well. The experimental and analytical axial force versus lateral displacement (perpendicular and parallel to the web at the middle of the member) curves for one of the members are given in Figure 9 and are seen to agree well. Tables 6 and 7 summarize the experimental and analytical findings regarding the strength of the members tested and analyzed under concentric and eccentric axial loads. The agreement is very good.

In addition to Z sections with 0°, 30°, 50° and 80° lip angles, which were considered in the experimental study, members with 10°, 20° and 40° lip angles were studied analytically. The results, compiled in Table 8, confirm the conclusion, drawn from experimental data, that there is no significant load capacity increase for lip angles greater than 30°. Also, as in the experiments, Z sections with lip angles less than 30° were were found to undergo substantial distortion, while, for lip angles greater than or equal to 30°, there was no discernible deformation of the cross section (see Figure 10). The distribution of von Mises stress along the members shows substantial fluctuations (see Figure 11(a)) for Z sections with lip angles less than 30°, indicative of

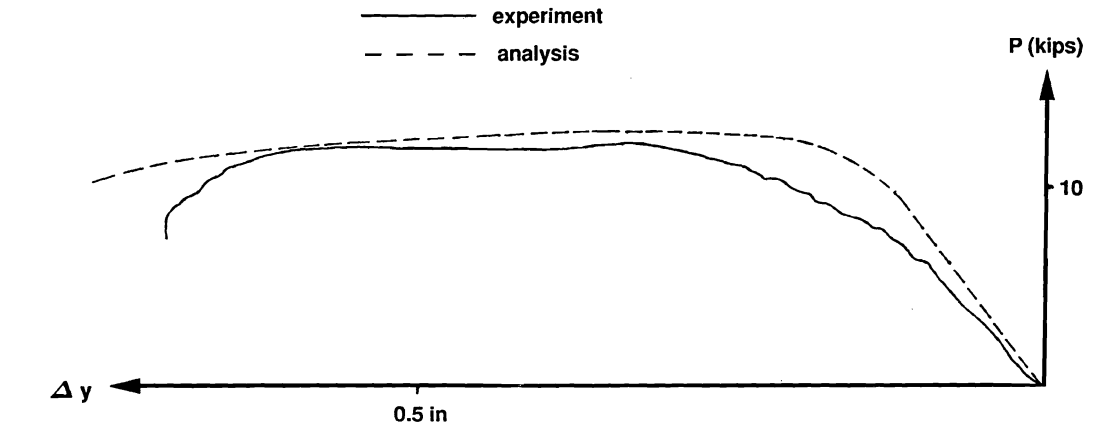

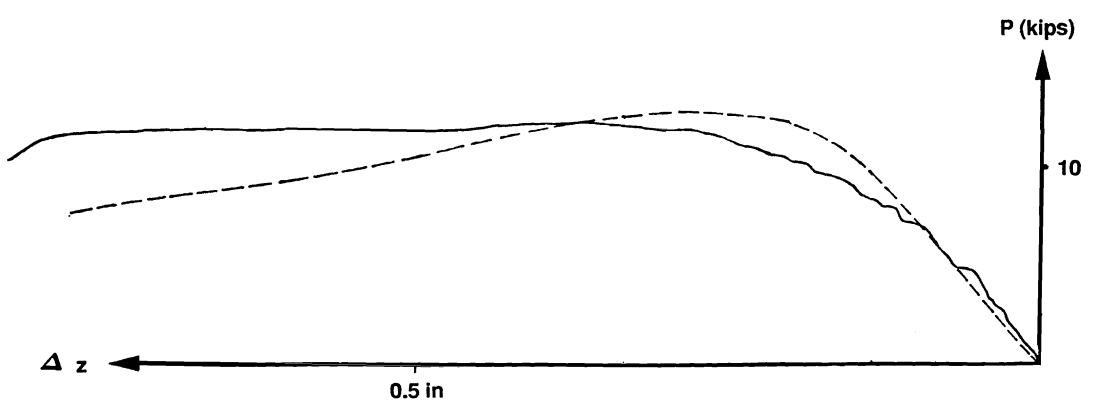

Figure 9: Axial load versus lateral displacements parallel to the web (Δ_z) and normal to the web (Δ_y) for $36in$ specimen ($F_y = 57.0ksi$) with 20° lip angle under eccentric load ($e_z = 2.0in$); experimental measurements and analytical calculations

Table 6: Analytical (F_y = 40.6 ksi) and experimental results

Length in	Lip Angle	Eccentricity e_z(in)	Ultimate Load	
			Experiments(kips)	Analysis(kips)
36.0	0°	0.0	22.35 & 23.35	23.43
	30°	0.0	32.50 & 32.80	30.96
	50°	0.0	35.05 & 35.25	31.84
		1.0	19.05	15.44
		2.0	12.70	10.70
	80°	0.0	35.80 & 32.90	32.09
60.0	0°	0.0	15.26 & 19.12	14.61
		1.0	10.89	11.30
		2.0	8.39	8.54
	30°	0.0	30.96	28.48
		1.0	12.50	11.59
		2.0	9.85	8.23
	50°	0.0	30.85 & 29.00	30.04
	80°	0.0	30.06 & 28.73	28.63
		1.0	13.64	11.89
		2.0	9.69	10.28
96.0	0°	0.0	11.31 & 10.10	9.63
	30°	0.0	16.44, 13.44, 13.69 & 14.79	11.82
		1.0	6.92	6.90
		2.0	5.46	5.06
	50°	0.0	14.46 & 14.147	12.10
	80°	0.0	15.55, 13.99 & 13.22	12.03

Table 7: Analytical (F_y = 57.0 ksi) and experimental results

Length in	Lip Angle	Eccentricity e_z(in)	Ultimate Load	
			Experiments(kips)	Analysis(kips)
60.0	30°	0.0	30.96	29.68
		1.0	12.50	13.66
		2.0	9.85	9.82
96.0	30°	0.0	16.44, 13.44, 13.69 & 14.79	11.96
		1.0	6.92	7.99
		2.0	5.46	6.21

deformation associated with local buckling. On the other hand, for lip angles greater than or equal to 30°, the longitudinal distribution of von Mises stress is practically uniform (Figure 11(b)).

Due to cold-working, the yield stress at the web-to-flange corners is higher than elsewhere in the Z section. The significance of this increased yield stress was examined analytically. It was found that, in members subjected to concentric loads, the additional strength at the corners is not utilized, while, under eccentric loads, there is only a slight increase in ultimate strength of the members. For example, neglecting the effect of higher corner yield stress, the load capacity of a $60in$ member with 0° lip angle subjected to an axial load with $2in$ eccentricity was calculated equal to $8.36kips$, compared with $8.54kips$ when the corner effect is considered, only a 2% increase. Thus, it is justifiable to neglect the cold-working increase in yield stress at the corners.

The sensitivity of the results to the yield stress of the material was assessed by analyzing a $60in$ member with 30° lips under both concentric and eccentric loads. The analysis was performed twice, first with yield stress equal to $40.6ksi$, then with yield stress equal to $57.0ksi$. Table 9 summarizes the results. The concentric load capacity increases by 4.5% for a 40.3% increase in yield stress, while the eccentric load capacities increase by 17.9% and 19.5% for eccentricities of $1.0in$ and $2.0in$, respectively. It should be noted that, in the absence of any initial imperfection, the peak concentric loads are not sufficiently high to cause yielding prior to buckling for the member considered. In the analysis, however, a small initial imperfection was applied for computational convenience (to convert the bifurcation point to a limit point). This imperfection is solely responsible for the (slight) influence of yield stress on the ultimate concentric load. Bending of the member under eccentric loads leads to yielding before the peak load is reached, and the yield stress has a substantial influence on the ultimate eccentric load.

The geometry of the Z section considered is such that the ultimate loads at eccentricities normal to the web (e_y) are lower than at equal eccentricities parallel to the web (e_z). Analytical results for eccentricities normal to the web, given in Table 10 along with the results for equal eccentricities parallel

Table 8: Analytical (F_y = 40.6 ksi) results

Length in	Lip Angle	Eccentricity in	Ultimate Load kips
36	10°	0.0	23.60
	20°	0.0	25.67
		$e_y = 1.0$	12.42
		$e_y = 2.0$	5.59
		$e_z = 1.0$	17.22
		$e_z = 2.0$	12.29
	40°	0.0	31.62
	50°	$e_y = 1.0$	13.40
		$e_y = 2.0$	6.48
60	0°	$e_y = 1.0$	8.45
		$e_y = 2.0$	5.91
	10°	0.0	17.99
	20°	0.0	22.80
	30°	$e_y = 1.0$	9.48
		$e_y = 2.0$	6.20
	40°	0.0	29.40
	80°	$e_y = 1.0$	10.03
		$e_y = 2.0$	6.88
96	10°	0.0	9.39
		$e_y = 1.0$	5.57
		$e_y = 2.0$	4.28
		$e_z = 1.0$	6.73
		$e_z = 2.0$	5.55
	20°	0.0	11.58
	40°	0.0	11.99
		$e_y = 1.0$	6.30
		$e_y = 2.0$	4.57
		$e_z = 1.0$	7.24
		$e_z = 2.0$	5.49

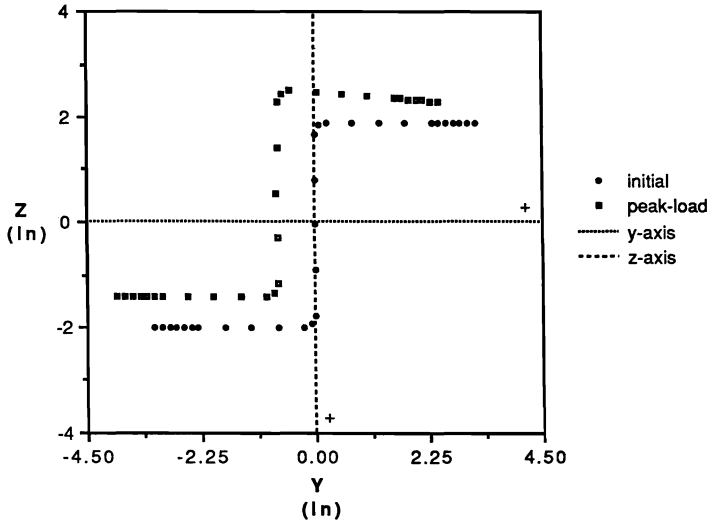

Figure 10 (a): Initial and deformed (at about peak load) cross sections; $60in$ specimen ($F_y = 40.6ksi$) with 0° lip angle

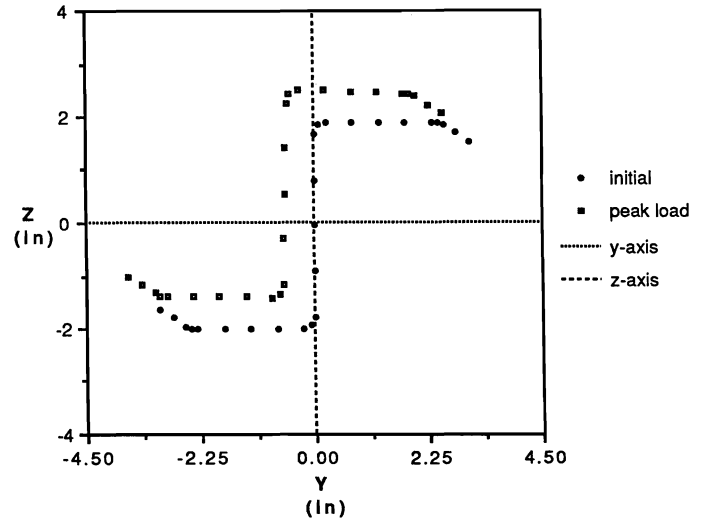

Figure 10 (b): Initial and deformed (at about peak load) cross sections; $60in$ specimen ($F_y = 40.6ksi$) with 30° lip angle

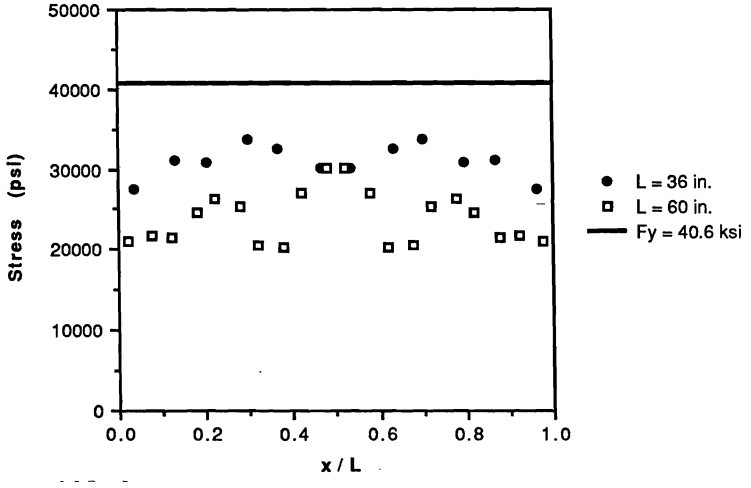

Figure 11 (a): Longitudinal distribution of von Mises stress in the flange at about peak load (concentric); $36in$ and $60in$ specimens ($F_y = 40.6ksi$) with 10° lip angle

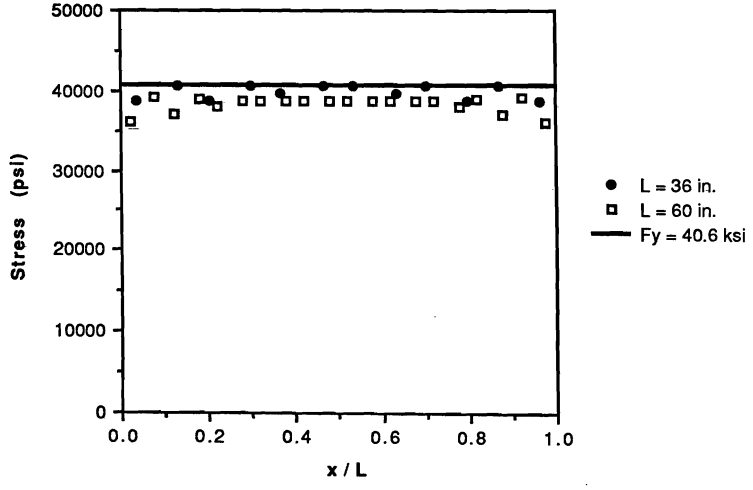

Figure 11 (b): Longitudinal distribution of von Mises stress in the flange at about peak load (concentric); $36in$ and $60in$ specimens ($F_y = 40.6ksi$) with 40° lip angle

Table 9: Ultimate load for different yield stresses

Specimen	Eccentricity	Max. Load	
		$F_y = 57.0$ksi	$F_y = 40.6$ksi
60 in, 30°	0.0 in.	29.75 kips	28.48 kips
	$e_z = 1.0$ in	13.66 kips	11.59 kips
	$e_z = 2.0$ in	9.82 kips	8.23 kips

to the web, confirm this fact. The differences appear to be most pronounced for short members, smaller lip angles (0° to 20°) and the larger of the two eccentricities considered. Additional results were obtained for the $60in$ specimen with 30° lip angle subjected to loads with combined eccentricities. It can be seen (Table 11) that eccentricity in one direction reduces the effect of eccentricity in the other direction.

The significance of initial imperfection was investigated analytically for several members (see Table 12). A sinusoidal imperfection was applied to each member with maximum displacement Δy at the middle of the member in the direction normal to the web. The results indicate that the stability of Z-section members (under concentric loads) is sensitive to the initial imperfection.

Table 10: Ultimate load for different eccentricities, parallel (e_z) and normal (e_y) to the web

Specimen Length	Lip Angle	Eccentricity	Max. Load
36 in.	20°	e_z = 1.0 in.	17.22 kips
(F_y = 40.6 ksi)		e_y = 1.0 in.	12.42 kips
		e_z = 2.0 in.	12.29 kips
		e_y = 2.0 in.	5.59 kips
36 in.	50°	e_z = 1.0 in.	15.44 kips
(F_y = 40.6 ksi)		e_y = 1.0 in.	13.40 Kips
		e_z = 2.0 in.	10.70 kips
		e_y = 2.0 in.	6.48 kips
60 in.	0°	e_z = 1.0 in.	11.30 kips
(F_y = 40.6 ksi)		e_y = 1.0 in.	8.45 kips
		e_z = 2.0 in.	8.54 kips
		e_y = 2.0 in.	5.91 kips
60 in.	30°	e_z = 1.0 in.	11.59 kips
(F_y = 40.6 ksi)		e_y = 1.0 in.	9.48 kips
		e_z = 2.0 in.	8.23 kips
		e_y = 2.0 in.	6.20 kips
60 in.	30°	e_z = 1.0 in.	13.66 kips
(F_y = 40.6 ksi)		e_y = 1.0 in.	10.36 kips
		e_z = 2.0 in.	9.82 kips
		e_y = 2.0 in.	6.59 kips
60 in.	80°	e_z = 1.0 in.	11.89 kips
(F_y = 40.6 ksi)		e_y = 1.0 in.	10.03 kips
		e_z = 2.0 in.	10.28 kips
		e_y = 2.0 in.	6.88 kips
96 in.	10°	e_z = 1.0 in.	6.73 kips
(F_y = 40.6 ksi)		e_y = 1.0 in.	5.57 kips
		e_z = 2.0 in.	5.55 kips
		e_y = 2.0 in.	4.28 kips
96 in.	40°	e_z = 1.0 in.	7.24 kips
(F_y = 40.6 ksi)		e_y = 1.0 in.	6.30 kips
		e_z = 2.0 in.	5.49 kips
		e_y = 2.0 in.	4.57 kips

Table 11: Ultimate load for combined eccentricities

Specimen	e_y(in)	e_z(in)	Max. Load
60in, 30°	0.0	0.0	30.96 kips
$F_y = 57.0$ksi	0.0	1.0	13.66 kips
	0.0	2.0	9.82 kips
	1.0	0.0	10.36 kips
	2.0	0.0	6.59 kips
	1.0	1.0	8.10 kips
	1.0	2.0	7.09 kips
	2.0	1.0	5.74 kips
	2.0	2.0	5.57 kips

Table 12: Sensitivity to initial imperfection

Specimen	Δy	Max. Load
60 in, 30°	0.010 in	29.68 kips
	-0.015 in	27.99 kips
	0.025 in	26.98 kips
60 in, 40°	0.010 in	29.40 kips
	-0.090 in	22.04 kips
60 in, 50°	0.010 in	30.04 kips
	-0.090 in	22.45 kips
60 in, 80°	0.010 in	28.63 kips
	-0.090 in	22.97 kips
96 in, 10°	-0.018 in	10.82 kips
	-0.118 in	9.39 kips

SUMMARY

In this work, experimental and analytical studies were conducted towards better understanding of the behavior of (cold-formed) Z-section steel members under concentric and eccentric axial loads. The main findings of this investigation can be summarized as follows:

1. The analytical technique developed in this work simulates the observed behavior of Z-section members very well.
2. The experimental results indicate and the analytical results confirm that the 1986 AISI Specification are overly conservative in estimating the load capacity of the Z section with 0° lip.
3. The experiments suggest and the analysis establishes beyond doubt that, for the Z section considered, lip angles greater than or equal to 30° ensure adequate stiffening against local and distortional buckling.
4. The increased yield stress at the web-to-flange corners has no effect on the ultimate concentric load and practically negligible effect under eccentric loads.
5. The ultimate eccentric loads are sensitive to the yield stress of the steel.
6. The stability of Z-section members (under concentric loads) is sensitive to initial imperfections.

APPENDIX. REFERENCES

Ahmad, S., Irons, B. M. and Zienkiewicz, O. C. (1970). "Analysis of Thick and Thin Shell Structures by Curved Finite Elements," *International Journal for Numerical Methods in Engineering*, pp. 419-451.

American Iron and Steel Institute (1986). *Cold-Formed Steel Design Manual.*

Needleman, A. (1982). "Finite Elements for Finite Strain Plasticity Problems," in *Plasticity of Metals at Finite Strain: Theory, Experiment and Computation*, edited by E. H. Lee and R. L. Mallett, Rensselaer Polytechnic Institute, Troy, New York, pp. 387-436.

Purnadi, R. W. (1990). "Experimental and Analytical Studies of Z-Section Steel Members Under Axial Loading," *Ph.D. Dissertation*, Department of Civil Engineering, The University of Texas, Austin, Texas.

Riks, E. (1984). "Some Computational Aspects of the Stability Analysis of Nonlinear Structures," *Computer Methods in Applied Mechanics and Engineering*, pp. 219-259.